Observation of spectrum effect on the measurement of intrinsic error field on EAST

2016 Nucl. Fusion 56 066011

(http://iopscience.iop.org/0029-5515/56/6/066011)

IOP Publishing | International Atomic Energy Agency Nuclear Fusion

Nucl. Fusion **56** (2016) 066011 (8pp) doi:10.1088/0029-5515/56/6/066011

Observation of spectrum effect on the measurement of intrinsic error field on EAST

Hui-Hui Wang[1], You-Wen Sun[1], Jin-Ping Qian[1], Tong-Hui Shi[1], Biao Shen[1], Shuai Gu[1], Yue-Qiang Liu[2], Wen-Feng Guo[1], Nan Chu[1], Kai-Yang He[1], Man-Ni Jia[1], Da-Long Chen[1], Min-Min Xue[1], Jie Ren[1], Yong Wang[1], Zhi-Cai Sheng[1], Bing-Jia Xiao[1], Zheng-Ping Luo[1], Yong Liu[1], Hai-Qing Liu[1], Hai-Lin Zhao[1], Long Zeng[1], Xian-Zu Gong[1], Yun-Feng Liang[1], Bao-Nian Wan[1] and The EAST Team

[1] Institute of Plasma Physics, Chinese Academy of Sciences, Hefei 230031, People's Republic of China
[2] CCFE Culham Science Centre, Abingdon, OX14 3DB, UK

E-mail: ywsun@ipp.ac.cn

Received 14 December 2015, revised 28 March 2016
Accepted for publication 12 April 2016
Published 25 May 2016

Abstract

Intrinsic error field on EAST is measured using the 'compass scan' technique with different $n = 1$ magnetic perturbation coil configurations in ohmically heated discharges. The intrinsic error field measured using a non-resonant dominated spectrum with even connection of the upper and lower resonant magnetic perturbation coils is of the order $b_{r2,1}/B_T \simeq 10^{-5}$ and the toroidal phase of intrinsic error field is around 60°. A clear difference between the results using the two coil configurations, resonant and non-resonant dominated spectra, is observed. The 'resonant' and 'non-resonant' terminology is based on vacuum modeling. The penetration thresholds of the non-resonant dominated cases are much smaller than that of the resonant cases. The difference of penetration thresholds between the resonant and non-resonant cases is reduced by plasma response modeling using the MARS-F code.

Keywords: intrinsic error field, non-resonant, spectrum analysis, EAST

(Some figures may appear in colour only in the online journal)

1. Introduction

Tokamak is designed to be toroidally symmetric. However, non-axisymmetric magnetic perturbations inevitably exist in the design and construction, such as field coil connection, misalignment, displacement and feedback of the conducting walls. These slight non-axisymmetric magnetic perturbations, known as intrinsic error field (IEF), can induce locked modes and loss of confinement, and especially can lead to disruption. Therefore, error fields and locked modes are of great concern in theoretical and experimental investigations.

To avoid the locked modes, a straightforward approach is to measure and correct the IEF. To date, the IEF measurement and correction relevant experiments have been carried out in many tokamaks, e.g. DIII-D [1–11], JET [12–14], COMPASS-C [2], MAST [15, 16], NSTX [17], Alcator C-Mod [18], TCV [19], ASDEX-Upgrade [20], TEXT-U [21] or J-TEXT [22], KSTAR [23], etc. The approaches on these devices can be classified into two groups: the direct measurement approach and the plasma response approach. The direct measurement approach was employed once in DIII-D [1], TCV [19] and ITER prediction [24, 25]. However, because of the complexity of error field sources, it is seldomly employed. Nevertheless, direct analysis on coil displacement and tilt may give instructions and predictions to the devices under engineering design and construction [24, 25]. The plasma response approach is an effective and convenient way. Therefore it plays a significant role in measuring and correcting the IEF in existing tokamaks. As one of the plasma response approaches [25], the 'compass scan' technique is an effective technique to measure

such small IEF [6, 7, 13, 15, 16] with an amplitude at about $b_r/B_T \sim 10^{-4}$–10^{-5}. This technique first requires the measurement error field penetration (or locked mode onset) thresholds of different toroidal phases of external resonant magnetic perturbation (RMP) coil currents, and then a fitted circle with the penetration thresholds and their toroidal phases. The shift of the center of the circle is the measured intrinsic error field. On the basis of IEF measurement with the 'compass scan' technique, error field correction has been succeeded in exploring the lower density region in some devices [6, 7, 15–17].

Further investigations indicate that IEF correction is still not well resolved. As the $n = 1$ error field couples to more than one surface in the ideal plasma response, there is only a 50% improvement in the low density locked mode limit from the $n = 1$ correction field in DIII-D [7]. Moreover the amplitude difference of error field correction coils (EFCCs) in JET with different phases nearly can be neglected [7], whereas earlier IEF measurement experiment using saddle coils shows a fairly good correction result [13]. The reason of the difference between the two experiments might be that the upgraded EFCCs have a more non-resonant spectrum than saddle coils in the previous JET device [26]. Furthermore, updated predictions of error field with locked mode theory requires at least a 50% correction in ITER [7]. Therefore error field correction is still a concern even in present devices. Besides, recent investigations on the measurement and correction of IEF shows that 'kink resonant' is crucial in DIII-D [8, 9, 27] and NSTX [27]. These show the significance of the non-resonant effect. Nonetheless, experiments in other devices are still significant to further verify this view. Therefore, experimental measurement of IEF is designed to investigate the RMP spectrum effect on EAST. Recently, spectrum effects on ELM control have also been observed in DIII-D [28, 29] and MAST [30]. Thus continuing spectrum effect investigations may also promote the understanding of ELM control with RMP.

In this paper, measurement of IEFs using different RMP spectra on EAST are presented in section 2. The spectrum effect on error field penetration is then presented in section 3. Finally, a summary and conclusion are given in section 4.

2. Measurement of intrinsic error field with different RMP coil configurations

The RMP system consists of two arrays of coils with up and down symmetry on EAST, as shown in figure 1. Eight uniformly distributed coils along the toroidal direction are comprised in each array. Each coil consists of 4 turns and the maximum current of the power supply is 2.5 kA. The EAST vacuum vessel consists of 16 ports, named as capital letters 'A, B, C,..., P'. Each coil covers toroidally two ports. The center of the coil covering P and A ports is defined as 0°. The RMP coils may be set as odd and even connection in the 2014 campaign on EAST. Even connection means that the toroidal phase difference between the upper and lower RMP coil currents (hereafter referred to as 'phase difference') $\Delta\phi = \phi_{\text{upper}} - \phi_{\text{lower}} = 0°$, while odd represents $\Delta\phi = \phi_{\text{upper}} - \phi_{\text{lower}} = 180°$. The characteristic of the $n = 1$

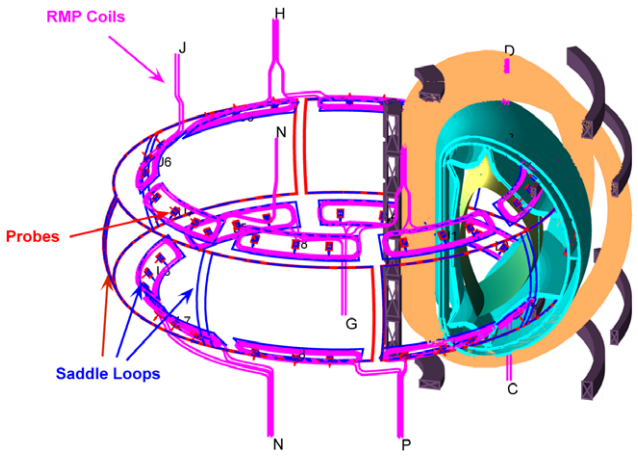

Figure 1. Positions of saddle loops and magnetic probes embed in RMP coils in EAST.

RMP vacuum spectra for these two configurations analyzed by MAPS code [31] are shown in figure 2. Figure 2(*a*) is for the even connection case, and figure 2(*b*) is for the odd one. The blue dashed line represents the 'pitch resonance', $m = nq$, and the length of the red line segments at different rational surfaces are the vacuum island widths for coil current $I_{\text{rmp}} = 1\ kA$. It is shown that the odd one has a much better pitch resonance. The odd one is a typical resonant dominant spectrum and the even one is a non-resonant dominant spectrum based on MAPS vacuum modeling.

Besides the existing magnetic diagnostics on EAST [32, 33], some new sensors have been installed in 2014 to give better three-dimensional information for RMP studies. Three arrays of saddle loops were installed at the upper, middle and lower planes of the low field side, as shown in figure 1. In the upper and lower planes, each saddle loop is placed close to each RMP coil(corresponding to the blue line in the upper and lower planes in figure 1). The midplane array consists of 12 *saddle loops* with 8 *smaller ones* and 4 *larger ones*. Each *smaller saddle loop* covers two midplane ports and each *larger one* covers four midplane ports. Two arrays of 2×24 probes are distributed inside the RMP loops.

To obtain accurate IEF, the experiments are carried out in well reproduceable lower single null ohmic plasmas with toroidal magnetic field, $B_T \simeq -1.75\ T$, plasma current, $I_P \simeq 460$ kA, safety factor of 95% flux surface, $q_{95} \simeq -3.5$ and fixed line averaged electron density, $\langle n_e \rangle \simeq 1.0 \times 10^{19}\ \text{m}^{-3}$. Here, negative q means the toroidal field is in the opposite direction to the toroidal plasma current, following the convinence in MAPS code [31]. The positive toroidal direction is defined as counter closewise from the top view. The global parameters are kept almost the same in the reproduceable target plasmas used in this paper (see figure 3 for example). The IEF is measured using the 'compass scan' technique [6, 7, 13, 15, 16] in the following. The RMP spectrum used for IEF measurement was often chosen as a 'better coupling one' [6, 7]. The field penetration thresholds for the even RMP configuration are typically much lower, which will be discussed later in detail in section 3. Therefore, we present the measurement of IEF with even RMP configuration at first in

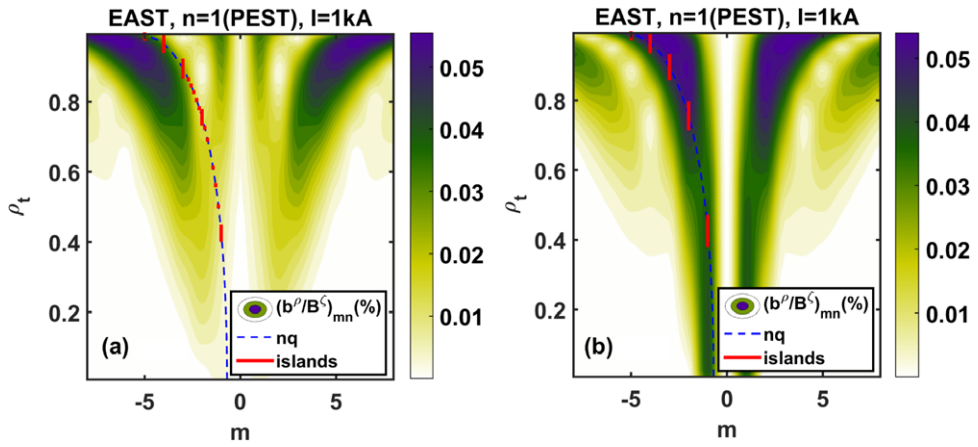

Figure 2. Spectra of $n = 1$ RMP with (a) even connection and (b) odd connection.

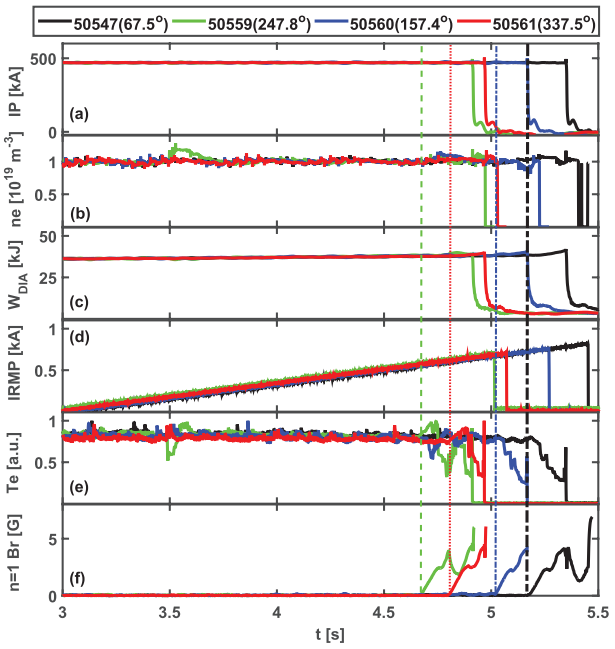

Figure 3. Penetration experiments with toroidal phases of RMP coil current $\phi = 67.5°, 247.8°, 157.4°, 337.5°$ in the even connection case. Temporal evolution of (a) plasma current, (b) line averaged electron density, (c) plasma stored energy, (d) RMP current amplitude, (e) electron temperature, (f) $n = 1$ radial magnetic perturbation from plasma. The verticle lines (bold dash–dotted line 50547, dashed line 50559, dash–dotted line 50560, dotted line 50561) represent the error field penetration moment when the $n = 1$ magnetic perturbation starts to increase.

section 2.1. To study the spectrum effect, the measured results with odd one are presented in section 2.2.

2.1. Intrinsic error field measurement with even connection of RMP coils

We first employ the even RMP coil configuration for the measurement of IEF. Four different toroidal phase discharges (RMP coil phases, $\phi = (67.5°, 247.8°, 157.4°, 337.5°)$, hereafer as 'toroidal phase') are carried out (figure 3). Figure 3 shows the typical time evolution of error field penetration. The plasma current is fixed at about 460 kA figure 3(a). The line averaged electron density measured by a hydrogen cyanide (HCN) laser interferometer (figure 3(b)) and stored energy measured from diamagnetic loops (figure 3(c)) are also given. Figures 3(a)–(c) indicate that the four shots are well reproduceable. Figure 3(d) is the slow ramping up of the RMP coil currents. Figure 3(f) is the $n = 1$ magnetic perturbation signals from the plasma measured from the midplane saddle loops. The penetration happens at the onset of the $n = 1$ magnetic perturbation indicated by the verticle lines. The penetration moment is also verified by the fast drop of electron temperature near the edge measured by electron cyclotron emission (ECE) diagnostics, as shown in figure 3(e). It is shown that penetration time and hence the thresholds are different at the four toroidal phases. The typical two-dimensional locked mode structure measured by the three arrays of saddle loops in the lower field side for *shot* 50561 is shown in figure 4. It shows a clear $n = 1$ mode structure. The dashed lines $q = -2$ and $q = -3$ indicate roughly the pitch angles of the perturbation from the $m/n = -2/1$ and $m/n = -3/1$ components, respectively. It is shown that the toroidal phase of the locked state is around 135 degrees, which approximates to the phase of the $-2/1$ or $-3/1$ rational surface. The toroidal penetration phases, RMP vacuum phases and vacuum thresholds for the four shots are summarized in table 1. It is shown that the penetration phases are consistent with the corresponding RMP vacuum phases of the $m = -2$ or $m = -3$ components. This means that the plasma is locked to the vacuum field frame after field penetration.

We can obtain the IEF from the penetration thresholds of the above four shots and some other repeated shots. By fitting the penetration thresholds of upper RMP coil peak currents and their corresponding toroidal phases with a circle, we can obtain the intrinsic error field, as shown in figure 5(a). The IEF amplitude with upper RMP coil peak current is about 87.1 A and the toroidal phase is about 267.9°. At different phase differences between upper and lower RMP coil currents, a set of upper or lower coils cannot reflect the whole information of the penetration RMP field, thus we then give the IEF using vacuum field penetration thresholds. By fitting the vacuum thresholds and toroidal phases of the $q = -2$ surface with a circle, we can obtain the intrinsic error field, as shown in figure 5(b). The amplitude of IEF is about $b_{r2/1} \sim 0.1$ G

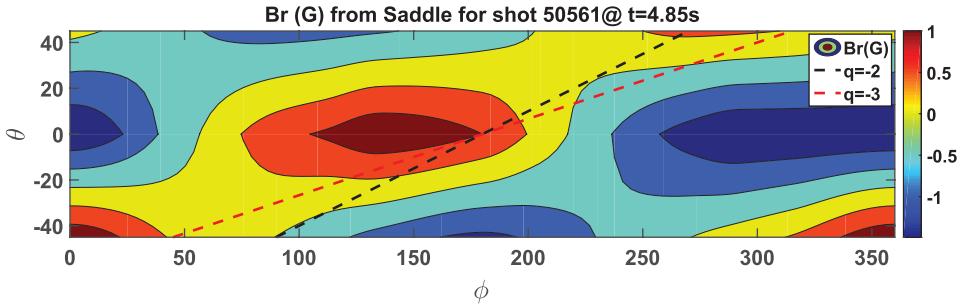

Figure 4. Two-dimensional structure of the magnetic perturbations from plasma after field penetration measured by the 3 groups of saddle loops in *shot* 50561.

Table 1. Toroidal phase of the plasma response field after field penetration and the phases of the $m/n = -2/1$ and $m/n = -3/1$ components of the vacuum RMP.

	$n = 1$ Vacuum threshold(phase)		
Shot	$m = -2$	$m = -3$	Penetration phase
50547	0.9078(227.2)	2.1183(234.1)	(225)
50559	0.7459(47.2)	1.7406(54.1)	(45)
50560	0.8509(317.2)	1.9856(324.1)	(340)
50561	0.7868(137.2)	1.8359(144.1)	(135)

($\simeq 6 \times 10^{-6} B_T$) and the toroidal phase is about 67.6°. If we fit the circle using the −3/1 component, the obtained intrinsic error field is about $b_{r3/1} \sim 0.2$ *G* ($\simeq 1.2 \times 10^{-5} B_T$) and the toroidal phase is about 74.5°. Both of these give an extremly small intrinsic error field level. This is helpful for extending the plasma operation window to low density at low q_{95} without error field correction.

2.2. Intrinsic error field measurement with odd connection of RMP coils

To study the RMP spectrum effect on error field penetration and the evaluation of IEF, the intrinsic error field measurement in the same target plasma is repeated with the odd connection of RMP coils. With the same technique, the IEF measured in the odd connection case is shown in figure 6. Figure 6(*a*) shows that the IEF amplitude with upper RMP coil peak current is about 172.4 *A* and the toroidal phase is about 153.6°. Figure 6(*b*) shows that the obtained IEF amplitude is about $b_{r2/1} \sim 0.7$ *G* ($\simeq 4 \times 10^{-5} B_T$) and the toroidal phase is 58.3°. The amplitudes of the even and odd ones are significantly different. However, the IEF phases are almost the same in both connection cases. The phase is also consistent with that of the natural locked mode. This means that the measurement itself is reliable.

2.3. Discussion

The obtained intrinsic error field is in general quite small, although the amplitudes are different for the two RMP configurations used. We have also tried to create the target plasma for error field correction study in ohmic discharge by ramping down of the plasma density during the plasma current flat top. However, it always enters runaway discharge before the natural penetration happens. This again confirms the small amplitude of the measured intrinsic error field. Besides the accurate manufacturing of the magnetic coils on EAST, the reasons for so small intrinsic error field might include the large distances between the poloidal field(PF) coils and the plasma (on the order of meters) limited by superconducting coils structure, and the relatively small contribution of the busbar of the toroidal field(TF) coil because there are 130 turns for each TF coil.

We have also tried to test the PF and TF coils contribution to the IEF. We have tried to apply the RMP field at different times of the plasma current flat top to test the central solenoidal PF coil contribution, because their currents have relatively large changes. No obvious difference has been observed. This means that they may not have a significant contribution. It is hard to test the contribution from the large PF coils for the vertical field, because they do not change much during the current flat top. In addition, we have also analyzed plasma intrinsic locked mode shots with opposite toroidal field directions. The difference of natural locked mode phases is less than 90°. Thus the toroidal field might contribute little to the IEF. However, direct measurement of the intrinsic error field using the magnetic sensors will be investigated in the near future.

3. Spectrum effect on error field penetration

Figures 5 and 6 not only indicate that the amplitude of IEF is different between even and odd connection cases, but also show that the penetration thresholds of the odd connection are much larger than those of the even connection (for the convenience of comparison, the fitted circle of figure 5 is shown as a dashed circle in figure 6). The reason for the large difference of vacuum −2/1 mode penetration thresholds between even and odd connections may be the spectrum effect. Figure 2 shows the even connection corresponds to non-resonant dominated spectrum, whereas the odd connection corresponds to resonant dominated spectrum. This is the fundamental difference in these two shots. Therefore, a reasonable explanation for the threshold difference is that the non-resonant perturbation spectrum has a significant effect on field penetration.

To further clarify the spectrum effect on error field penetration, a scan of phase difference ($\Delta\phi$) of upper and lower

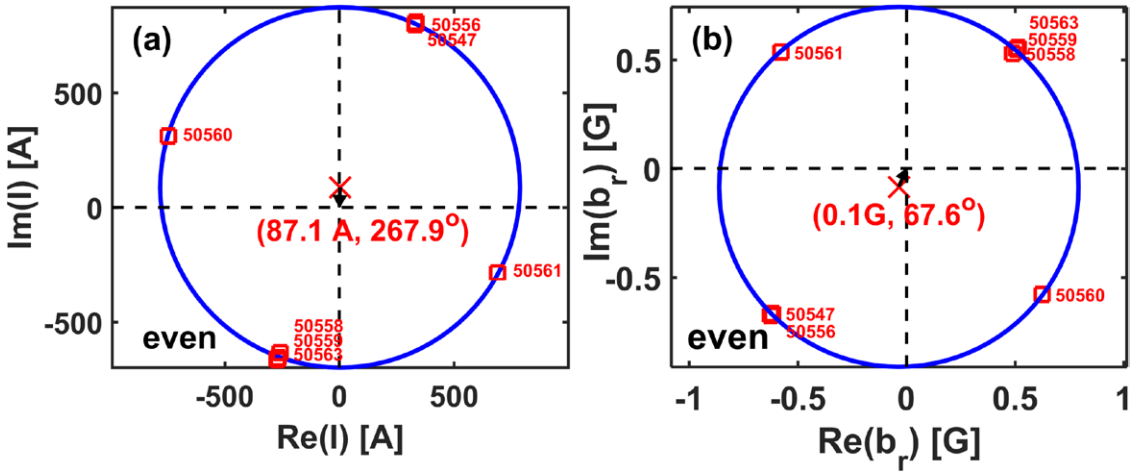

Figure 5. Fitting of the intrinsic error field in the even connection case (*a*) under penetration threshold of upper RMP coil peak current, (*b*) under $-2/1(m/n)$ vacuum resonant field amplitude on the rational surface at the penetration moment. Red squares are penetration thresholds for different shots and the red cross is the fitted center of the circle. The black arrow represents the final evaluated intrinsic error field.

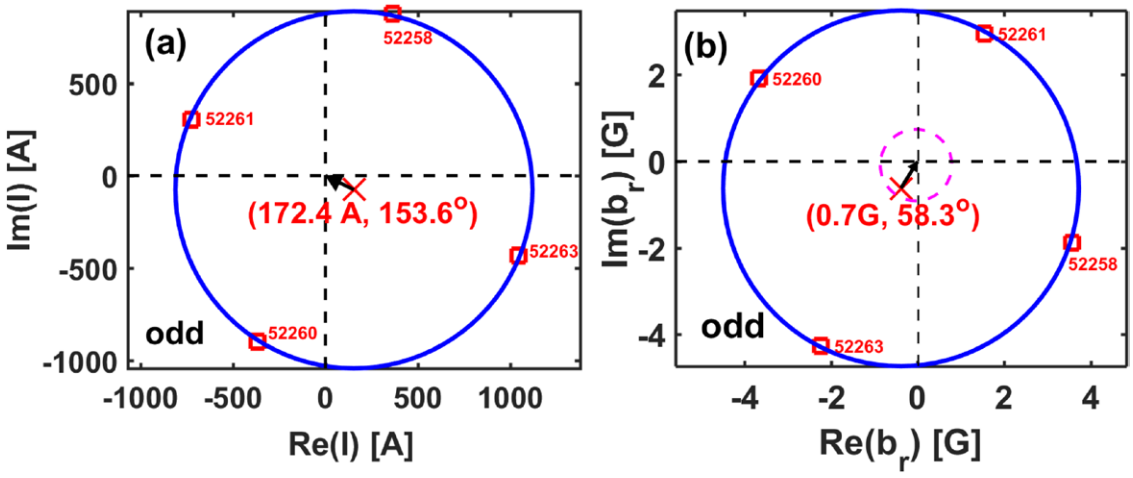

Figure 6. The same plot as figure 5 for the evaluated intrinsic error field using the odd RMP coil configuration. The dashed circle represents the solid circle in figure 5(*b*).

RMP coil currents in different shots was carried out in the 2015 spring experiment campaign on EAST. Figure 7 shows the penetration thresholds of the shots with $\Delta\phi = 180°$, 90° and 45°. It shows that fields are penetrated at different times in *shot* 55296(180°) and *shot* 55447(45°), while no penetration happens in *shot* 55312(90°) at the maximum RMP current 2.5 kA (e.g. stars under the shadow region in figure 8). This suggests that the field penetration threshold strongly depends on the RMP spectrum. The dependence of field penetration threshold on the phase difference is shown in figure 8. The solid line corresponds to the strength of vacuum $-2/1$ (figure 8(*a*), $-3/1$ in figure 8(*b*)) component at the $q = -2$ ($q = -3$) rational surface with the maximum RMP current 2.5 kA, while circles represent penetration thresholds of the $-2/1$ ($-3/1$) resonant component. Figure 8(*c*) gives the RMP peak current of penetration threshold. If the valley of vacuum modeling curve corresponds to the peak threshold, then threshold field of vacuum modeling will be close to alignment. Comparing the solid line in figure 8(*a*) and the symbols in figure 8(*c*), there is about an 80 degree phase difference to match. Besides, figure 8 shows that the resonant dominated cases (at the phases about 180° and 225°) have larger penetration thresholds than the non-resonant cases (e.g. at 0° or 45°). Therefore, the spectrum indeed has a significant effect on error field penetration.

In the recent years, plasma response modeling has been of great concern [6, 8, 27, 29, 34, 35]. To further check this viewpoint, the plasma response based on the MARS-F code under the plasma equilibrium configuration of the above discharges is given in figure 9. Solid lines in figures 9(*a*) and (*b*) are the plasma response calculation result of $m/n = -2/1$ and $m/n = -3/1$ components at the corresponding rational surfaces, respectively. They represent the sum of vacuum field and response field. The amplitudes of circles in figure 9(*a*) are closer than that in figure 8(*a*), indicating the plasma response may interpret the difference of IEF derived by vacuum modeling. The penetration threshold of plasma response of $m/n = -3/1$ resonant component is better than that of the $m/n = -3/1$ resonant component. Comparing the solid line in figure 9(*a*) and symbols in figure 8(*c*), there is about a 45 degree phase difference to match.

By artificially shifting the plasma response curve back 45 degrees at the phase difference coordinate, it is found

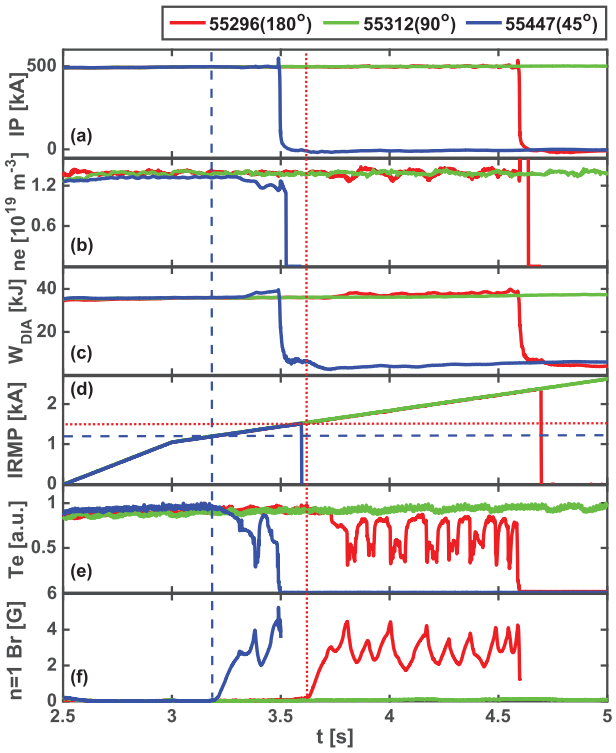

Figure 7. Penetration experiments with upper-lower phase differences $\Delta\phi = 180°(55296), 90°(55312), 45°(55447)$. Temporal evolution of (a) plasma current, (b) line averaged electron density, (c) plasma stored energy, (d) RMP coil current amplitude, (e) electron temperature near the edge, (f) $n = 1$ magnetic perturbation signal. The verticl lines (dotted line 55296, dashed line 55447) represent the error field penetration moment.

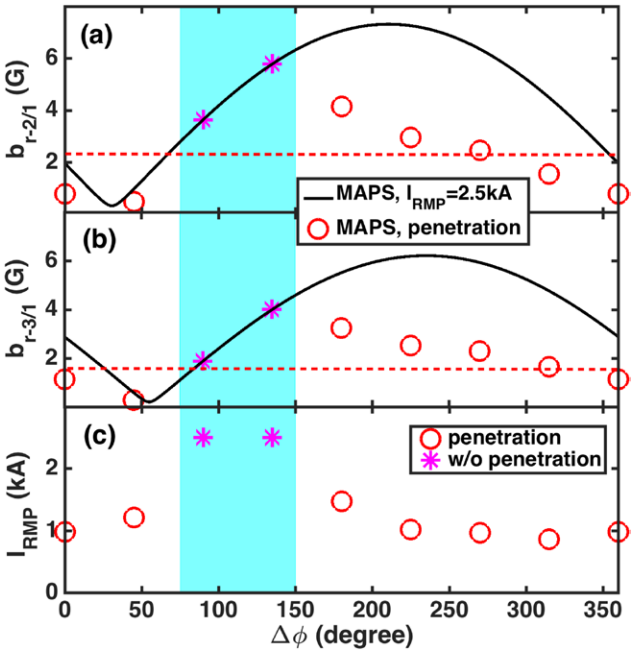

Figure 8. Dependence of $-2/1$ threshold field (a),$-$ 3/1 threshold field (b) and current (c) of error field penetration on $\Delta\phi$. The solid line is the vacuum $-2/1$ ($-3/1$) field amplitude at $q = -2$ ($-3/1$) rational surface analyzed by MAPS code with the maximum $n = 1$ RMP coil current at 2.5 kA. Circles are the error field penetration thresholds while stars correspond to no penetration when the maximum $n = 1$ RMP coil current is at 2.5 kA.

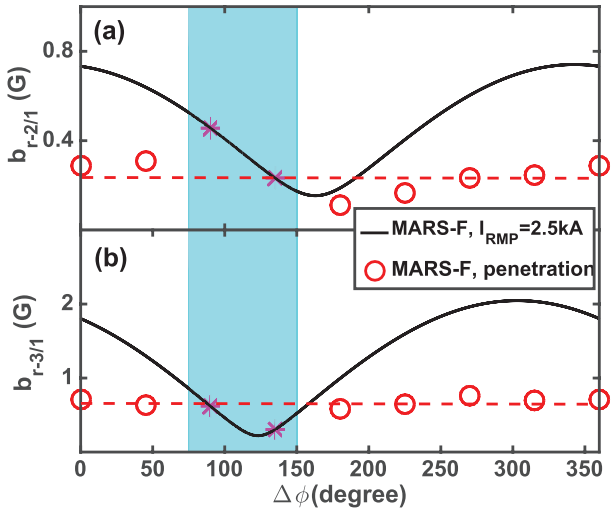

Figure 9. Dependence of $-2/1$ threshold field (a) and $-3/1$ threshold field (b) of error field penetration on $\Delta\phi$ as in figures 8(a) and (b). The difference is these threshold fields are derived from plasma response modeling using the MARS-F code.

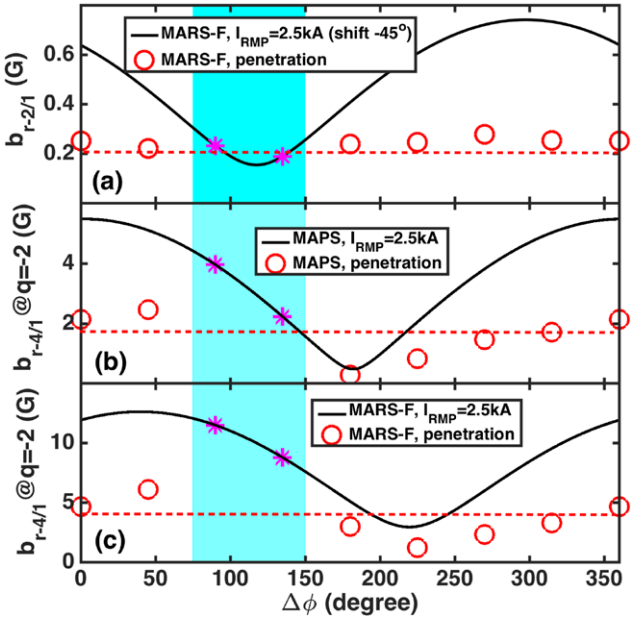

Figure 10. Dependence of $-2/1$ threshold field (a), vacuum $-4/1$ threshold field at $q = -2$ rational surface (b) and plasma response $-4/1$ threshold field at $q = -2$ rational surface (c) of error field penetration on $\Delta\phi$. (a) artificially shifting -45 degree relative to the MARS-F calculation results in figure 9(a).

that penetration thresholds are nearly the same as seen in figure 10(a). The underlying physics is not clear. By roughly calculating the IEF under the artificially shifting plasma response, by comparing IEF under vacuum field and the ratio of plasma response field amplitude to vacuum field amplitude at the corresponding phase difference, we can obtain that the IEF amplitude is about 0.032 G and 0.041 G in even and odd connection cases, respectively. This further indicates that IEF under the plasma response has a smaller difference. Thus plasma response modeling is a good candidate to make up the difference of IEF amplitude and penetration threshold

between the non-resonant dominated even connection case and resonant dominated odd connection case based on the vacuum modeling.

There is also a possibility that non-resonant components dominate the physical process of field penetration directly, and therefore inducing the difference of IEFs. To check the non-resonant component, we choose the $m/n = -4/1$ component at the $q = -2$ rational surface (figure 10(*b*)), which is the largest component in the most $\Delta\phi$ region, to make clear whether the non-resonant component dominates or not. It shows a large difference between the valley of $m/n = -4/1$ non-resonant vacuum field curve and RMP peak current. We have also checked the plasma response of the $m/n = -4/1$ component at the $q = -2$ rational surface, the difference is larger. Therefore, non-resonant components cannot dominate the physical process of field penetration directly.

The conventional RMP effect in the locked mode or penetration physics originates from the resistivity or other non-ideal terms in Ohm's law and is known for its flux averaged electromagnetic torque at the rational surface, i.e. second order electromagnetic torque $T_{\rm EM} = \langle \boldsymbol{\delta J} \times \boldsymbol{\delta B} \rangle$, which peaks just like the delta function distributed at the rational surface, hindering the plasma rotation against the viscous torque $T_{\rm VS}$. The penetration regimes and thresholds are thus derived by torque balance $T_{\rm EM} + T_{\rm VS} = 0$. It is known that the non-resonant magnetic perturbation may induce the braking of the plasma rotation [26, 36–38] because of the neoclassical toroidal viscosity (NTV) [39] effect. It will contribute additional torque in the torque balance equation. This may influence the field penetration by changing the plasma rotation [40]. According to the ideal plasma response theory, the $n = 1$ kink-resonant component around the $m > nq$ spectrum couples to the least stable mode [8, 27, 29, 34]. Once the ideal plasma response amplifies the non-resonant field, it can enhance the NTV effect. This might be the reason why the plasma response modeling cannot well interpret the field penetration. Furthermore, the field penetration process itself includes complex nonlinear behavior. To fully understand the non-resonant components effect on penetration needs self-consistent nonlinear modeling of plasma response, which is still an unsolved problem [41].

4. Summary and conclusion

Intrinsic error field on EAST is measured using the 'compass scan' technique with different $n = 1$ magnetic perturbation coil configurations in ohmically heated discharges. The intrinsic error field measured with even connection of upper and lower RMP coil currents is about $b_{r2,1} \sim 0.1G (\simeq 0.6 \times 10^{-5} B_{\rm T})$ and the toroidal phase is about 67.6°. By vacuum spectrum analysis, it shows that non-resonant components dominate at the rational surfaces in the even connection, while resonant components dominate at the rational surfaces in the odd one. The reasons for so small intrinsic error field might include the accurate manufacturing of the magnetic coils, the large distances between the poloidal field coils and the plasma (on the order of meters) limited by superconducting coils structure, and the relatively small contribution of the busbar of the toroidal field coil. The small IEF is good for accessing the lower density operation. It is found that penetration threshold and IEF have a dependence on spectrum structure. We have also measured the IEF with odd connection of upper and lower RMP coil currents. The toroidal phases of the intrinsic error field are both about 60°. The amplitude of the measured error field increased by a factor of 7, although it is still quite small. Furthermore, we have also tried to create the target plasma for error field correction study in ohmic discharge by ramping down the plasma density during the plasma current flat top. However, it always enters runaway discharge before the natural penetration happens. This again confirms the small amplitude of the measured intrinsic error field. In addition, we have also tried to find the sources of the IEF. The central solenoidal PF coils and toroidal field coils might have little to contribute to the IEF. It is hard to test the contribution from the large PF coils for the vertical field. However, direct measurement of the intrinsic error field using the magnetic sensors will be investigated in the near future.

The scanning of phase difference of upper and lower RMP coil currents are also shown to clarify the significance of non-resonant component on field penetration. The penetration thresholds in non-resonant dominated cases are much smaller than those in resonant dominated ones, which means that the non-resonant component plays an important role in field penetration. The plasma response on the basis of the MARS-F code is given to further understand the non-resonant physics. It is verified that linear response modeling is a good candidate for error field physics, although the result has about a 45 degree mismatch from the side of the $m/n = -2/1$ resonant component, whereas there is a good match from the side of the $m/n = -3/1$ resonant component. Generally, the field penetration process itself includes complex nonlinear behavior. To fully understand the non-resonant components effect on penetration needs self-consistent nonlinear modeling of plasma response, which is still an unsolved problem. In the future, carrying on continuing experimental investigations against theories and simulation on the non-resonant effect under various situations may provide more valuable information for ITER with varieties of magnetic perturbation spectra characteristics.

Acknowledgments

This work is supported by the National Magnetic Confinement Fusion Science Program of China under Grant No. 2013GB102000 and No. 2012GB105000, the National Natural Science Foundation of China under Grant No. 11205199, No. 11475224, No. 11505235 and No. 11475002, and the China Postdoctoral Science Foundation funded project under Grant No.2015M580557.

References

[1] La Haye R.J. and Scoville J.T. 1991 *Rev. Sci. Instrum.* **62** 2146
[2] La Haye R.J., Fitzpatrick R., Hender T.C., Morris A.W., Scoville J.T. and Todd T.N. 1992 *Phys. Fluids* B **4** 2098
[3] Garofalo A.M., La Haye R.J. and Scoville J.T. 2002 *Nucl. Fusion* **42** 1335
[4] Scoville J.T. and Haye R.J.L. 2003 *Nucl. Fusion* **43** 250

[5] Luxon J.L., Schaffer M.J., Jackson G.L., Leuer J.A., Nagy A., Scoville J.T. and Strait E.J. 2003 *Nucl. Fusion* **43** 1813
[6] Park J.K., Schaffer M.J., La Haye R.J., Scoville T.J. and Menard J.E. 2011 *Nucl. Fusion* **51** 023003
[7] Buttery R.J. *et al* and The DIII-D Team 2012 *Phys. Plasmas* **19** 056111
[8] Paz-Soldan C., Buttery R.J., Garofalo A.M., Hanson J.M., Haye R.J.L., Lanctot M.J., Park J.K., Solomon W.M. and Strait E.J. 2014 *Nucl. Fusion* **54** 073013
[9] Paz-Soldan C., Lanctot M.J., Logan N.C., Shiraki D., Buttery R.J., Hanson J.M., La Haye R.J., Park J.-K., Solomon W.M. and Strait E.J. 2014 *Phys. Plasmas* **21** 072503
[10] Shiraki D., Haye R.J.L., Logan N.C., Strait E.J. and Volpe F.A. 2014 *Nucl. Fusion* **54** 033006
[11] Shiraki D., Paz-Soldan C., Hanson J.M., Haye R.J.L., Logan N.C., Olofsson K.E.J., Strait E.J., Sweeney R.M. and Volpe F.A. 2015 *Plasma Phys. Control. Fusion* **57** 025016
[12] Fishpool G.M. and Haynes P.S. 1994 *Nucl. Fusion* **34** 109
[13] Buttery R.J., De' Benedetti M., Hender T.C. and Tubbing B.J.D. 2000 *Nucl. Fusion* **40** 807
[14] Lazzaro E. *et al* and contributors to the EFDA-JET work programme 2002 *Phys. Plasmas* **9** 3906
[15] Howell D.F., Hender T.C. and Cunningham G. 2007 *Nucl. Fusion* **47** 1336
[16] Kirk A., Liu Y., Martin R., Cunningham G., Howell D. and The Mast Team 2014 *Plasma Phys. Control. Fusion* **56** 104003
[17] Menard J.E. *et al* and The NSTX Research Team 2010 *Nucl. Fusion* **50** 045008
[18] Wolfe S.M. *et al* 2005 *Phys. Plasmas* **12** 056110
[19] Piras F., Moret J.M. and Rossel J.X. 2010 *Fusion Eng. Des.* **85** 739
[20] Maraschek M. *et al* and ASDEX Upgrade Team 2013 *40th EPS Conf. on Plasma Physics* P4.127 (Espoo, 2013)
[21] Craven W.A. and Wootton A.J. 1998 *Nucl. Fusion* **38** 585
[22] Rao B., Ding Y.H., Yu K.X., Jin W., Hu Q.M., Yi B., Nan J.Y., Wang N.C., Zhang M. and Zhuang G. 2013 *Rev. Sci. Instrum.* **84** 043504
[23] In Y., Park J.K., Jeon J.M., Kim J. and Okabayashi M. 2015 *Nucl. Fusion* **55** 043004
[24] Leuer J.A., La Haye R.J., Kellman A.G., Humphreys D.A., Scoville J.T., Gribov Y., Wesley J.C., Hender T.C. and Doinikov N. ITER asymmetric error fields and their correction *17th IEEE/NPSS Symp. on Fusion Engineering (San Diego, CA, 1997)* vol 1 pp 505–8
[25] Strait E.J. *et al* 2014 *Nucl. Fusion* **54** 073004
[26] Sun Y. *et al* and JET-EFDA contributors 2012 *Nucl. Fusion* **52** 083007
[27] Park J.K., Schaffer M.J., Menard J.E. and Boozer A.H. 2007 *Phys. Rev. Lett.* **99** 195003
[28] Wade M.R. *et al* 2015 *Nucl. Fusion* **55** 023002
[29] Paz-Soldan C. *et al* 2015 *Phys. Rev. Lett.* **114** 105001
[30] Liu Y., Kirk A., Gribov Y., Gryaznevich M.P., Hender T.C. and Nardon E. 2011 *Nucl. Fusion* **51** 083002
[31] Sun Y., Liang Y., Qian J., Shen B. and Wan B. 2015 *Plasma Phys. Control. Fusion* **57** 045003
[32] Shen B., Liu D.-M., Wang Y. and Du X.-Y. 2009 *Nucl. Fusion Plasma Phys.* (in Chinese) **29** 178
[33] Liu G.J., Wan B.N., Sun Y.W., Xiao B.J., Wang Y., Luo Z.P., Qian J.P. and Liu D.M. 2013 *Rev. Sci. Instrum.* **84** 073502
[34] Lanctot M.J. *et al* 2011 *Phys. Plasmas* **18** 056121
[35] Liu Y., Kirk A., Thornton A.J. and The Mast Team 2014 *Plasma Phys. Control. Fusion* **56** 104002
[36] Zhu W. *et al* 2006 *Phys. Rev. Lett.* **96** 225002
[37] Cole A.J., Callen J.D., Solomon W.M., Garofalo A.M., Hegna C.C., Lanctot M.J., Reimerdes H. and The DIII-D Team 2011 *Phys. Rev. Lett.* **106** 225002
[38] Garofalo A.M., Burrell K.H., DeBoo J.C., deGrassie J.S., Jackson G.L., Lanctot M., Reimerdes H., Schaffer M.J., Solomon W.M. and Strait E.J. 2008 *Phys. Rev. Lett.* **101** 195005
[39] Shaing K.C. 2003 *Phys. Plasmas* **10** 1443
[40] Cole A.J., Hegna C.C. and Callen J.D. 2007 *Phys. Rev. Lett.* **99** 065001
[41] Turnbull A.D. *et al* 2013 *Phys. Plasmas* **20** 056114